drolysis, permitting the measurement of VLDL production (*20*). VLDL production was increased 140% in *ob/ob* mice relative to lean controls (Fig. 4C, $P < 0.05$). Compared with *ob/ob* controls, VLDL production was reduced 72% in ab^J/ab^J; *ob/ob* mice (8.2 mg/dl per min versus 2.3 mg/dl per min, $P < 0.02$) (Fig. 4C).

These data show that SCD-1 is required for the fully developed obese phenotype of *ob/ob* mice and suggest that a significant proportion of leptin's metabolic effects may result from inhibition of this enzyme. The basis for the metabolic effects of SCD-1 deficiency is not known. One possibility is that reduced activity of SCD-1 may decrease adiposity by decreasing cellular levels of malonyl CoA, thereby reducing fatty acid biosynthesis and de-repressing fatty acid oxidation. In the absence of SCD-1, a reduced rate of triglyceride and VLDL synthesis increases the intracellular pool of saturated fatty acyl CoAs leading to an increase in fatty acid oxidation. Monounsaturated fats are necessary for normal rates of triglyceride and cholesteryl ester synthesis, which are required for hepatic lipid storage and VLDL synthesis (*19*). Saturated fatty acyl CoAs, but not monounsaturated fatty acyl CoAs, potently allosterically inhibit acetyl-CoA carboxylase (ACC), reducing cellular levels of malonyl CoA (*21, 22*). Malonyl CoA is required for fatty acid biosynthesis and also inhibits the mitochondrial carnityl palmityl transferase shuttle system, the rate-limiting step in the import and oxidation of fatty acids in mitochondria (*23*). This putative mechanism is similar to that described in mice lacking acetyl-CoA carboxylase 2, which also have increased fatty acid oxidation in skeletal muscle and a lean phenotype (*24*). The mechanism by which leptin increases fatty acid oxidation in liver may be similar to that in skeletal muscle in that both may operate by reducing ACC activity. However, in skeletal muscle, leptin—acting directly and indirectly via the CNS—inhibits ACC via α2 AMP-kinase, which phosphorylates and inhibits ACC (*25*).

Alternative mechanisms could also account for the metabolic effects of SCD-1 deficiency. Changes in SCD-1 activity could alter the levels of ligands for peroxisome proliferator–activated receptors PPARα and PPARγ, or other nuclear hormone receptors. Changes in the ratio of saturated to unsaturated fatty acids in phospholipids can also alter membrane fluidity, which could affect signal transduction. The observed increase in energy expenditure associated with SCD-1 deficiency also suggests that uncoupling activity and/or futile cycles are induced.

The effects of leptin on SCD-1 in liver are likely to require central action, as mice lacking the leptin receptor in brain have enlarged, fatty livers, whereas livers of mice with a liver-specific knockout of the leptin receptor appear normal (*26*). Leptin also reduces hepatic SCD-1 activity when administered intracerebroventricularly (*27*). The CNS signals that modulate liver metabolism in response to leptin are unknown. SCD-1 deficiency also appears to modulate CNS pathways that regulate food intake, perhaps secondary to the increased oxygen consumption.

Leptin may also modulate the production of monounsaturated fatty acids in tissues other than liver. Down-regulation of SCD enzyme activity by leptin in other tissues, including brain, could contribute to some of the observed metabolic effects. Although SCD-1 is the only isoform normally expressed in liver, both SCD-1 and SCD-2, a similar enzyme, are expressed in most other tissues. Both enzymes catalyze the same reaction, but their cellular distribution and substrate preferences may be different.

In summary, a deficiency of SCD-1 ameliorates the obesity of *ob/ob* mice and completely corrects the hypometabolic phenotype of leptin deficiency. These findings suggest that leptin-specific down-regulation of SCD-1 is an important component of the novel metabolic response to leptin and suggests that inhibition of SCD-1 could be of benefit for the treatment of obesity, hepatic steatosis, and other metabolic disorders.

References and Notes

1. Y. Zhang *et al.*, *Nature* **372**, 425 (1994).
2. J. M. Friedman, *Nature* **404**, 632 (2000).
3. S. Kamohara, R. Burcelin, J. L. Halaas, J. M. Friedman, M. J. Charron, *Nature* **389**, 374 (1997).
4. N. Levin, C. Nelson, A. Gurney, R. Vandlen, F. de Sauvage, *Proc. Natl. Acad. Sci. U.S.A.* **93**, 1726 (1996).
5. J. L. Halaas *et al.*, *Science* **269**, 543 (1995).
6. M. A. Pelleymounter *et al.*, *Science* **269**, 540 (1995).
7. L. A. Campfield, F. J. Smith, Y. Guisez, R. Devos, P. Burn, *Science* **269**, 546 (1995).
8. I. Farooqi *et al.*, *N. Engl. J. Med.* **341**, 879 (1999).
9. I. Shimomura, R. E. Hammer, S. Ikemoto, M. S. Brown, J. L. Goldstein, *Nature* **401**, 73 (1999).
10. E. A. Oral *et al.*, *N. Engl. J. Med.* **346**, 570 (2002).
11. Materials and methods are available as supporting material on *Science* Online.
12. A. Soukas, P. Cohen, N. D. Socci, J. M. Friedman, *Genes Dev.* **14**, 963 (2000).
13. J. M. Ntambi *et al.*, *J. Biol. Chem.* **263**, 17291 (1988).
14. J. M. Ntambi, *J Lipid Res.* **40**, 1549 (1999).
15. C.-P. Liang, A. R. Tall, *J. Biol. Chem.* **276**, 49066 (2001).
16. A. W. Ferrante, M. Thearle, T. Liao, R. L. Leibel, *Diabetes* **50**, 2268 (2001).
17. A. H. Gates, M. Karasek, *Science* **148**, 1471 (1965).
18. Y. Zheng *et al.*, *Nature Genet.* **23**, 268 (1999).
19. M. Miyazaki, Y.-C. Kim, M. P. Gray-Keller, A. D. Attie, J. M. Ntambi, *J. Biol. Chem.* **275**, 30132 (2000).
20. M. Merkel *et al.*, *J. Clin. Invest.* **102**, 893 (1998).
21. J. J. Volpe, P. R. Vagelos, *Physiol. Rev.* **56**, 339 (1976).
22. M. A. Lunzer, J. A. Manning, R. K. Ockner, *J. Biol. Chem.* **252**, 5483 (1977).
23. J. D. McGarry, G. P. Mannaerts, D. W. Foster, *J. Clin. Invest.* **60**, 265 (1977).
24. L. Abu-Elheiga, M. M. Matzuk, K. A. H. Abo-Hashema, S. J. Wakil, *Science* **291**, 2613 (2001).
25. Y. Minokoshi *et al.*, *Nature* **415**, 339 (2002).
26. P. Cohen *et al.*, *J. Clin. Invest.* **108**, 1113 (2001).
27. E. Asilmaz *et al.*, unpublished observation.
28. We thank K. Mao for help with lipid quantification; T. Scase for assistance with liver histology; J. Breslow for valuable discussions and critical reading of this manuscript; E. Asilmaz, M. Ishii, J. Montez, S. Novelli, and S. Pinto for critical reading of this manuscript; and S. Korres for assistance in preparing this manuscript. Supported by NIH Medical Scientist Training Program grant GM07739 (P.C.), the American Heart Association and Xenon Genetics, Inc. (J.M.N.), and NIH grant R01-DK41096 (J.M.F.).

Supporting Online Material

www.sciencemag.org/cgi/content/full/297/5579/240/DC1
Materials and Methods
Figs. S1 and S2
Tables S1 and S2

3 March 2002; accepted 14 May 2002

Multiple Roles of *Arabidopsis VRN1* in Vernalization and Flowering Time Control

Yaron Y. Levy,* Stéphane Mesnage,*† Joshua S. Mylne, Anthony R. Gendall,‡ Caroline Dean§

***Arabidopsis VRN* genes mediate vernalization, the process by which a long period of cold induces a mitotically stable state that leads to accelerated flowering during later development. *VRN1* encodes a protein that binds DNA in vitro in a non–sequence-specific manner and functions in stable repression of the major target of the vernalization pathway, the floral repressor *FLC*. Overexpression of *VRN1* reveals a vernalization-independent function for *VRN1*, mediated predominantly through the floral pathway integrator *FT*, and demonstrates that VRN1 requires vernalization-specific factors to target *FLC*.**

Many annual plants use seasonal variations in temperature and photoperiod to control the transition to flowering (*1*). Long periods of cold temperature (1 to 3 months of about 4°C) accelerate flowering later in development in a process known as vernal-

ization. In *Arabidopsis*, the pathways that regulate vernalization requirement and response converge on *FLC*, a gene encoding a MADS-box repressor protein. In vernalization-responsive genotypes, reduction in the abundance of *FLC* mRNA, protein, and time to flower is closely correlated with the duration of cold treatment (*2*, *3*). The activity of genes in the autonomous floral promotion pathway (*FCA*, *FY*, *FVE*, *FPA*, and *LD*) also reduces *FLC* RNA levels (*3*, *4*). Mutations in these genes confer *FLC*-mediated late flowering, which is reversed by vernalization to early flowering. Recent work suggests that the activity of the autonomous, photoperiod, and vernalization pathways is integrated by common downstream targets, including *AGL20* and *FT*, and that FLC represses flowering by negatively regulating these genes (*5*, *6*).

The molecular basis of vernalization has been investigated through characterization of a set of genes (*VRN* genes) defined by mutations that reduce the vernalization response (*7*). We recently showed that one of these genes, *VRN2*, encodes a nuclear-localized zinc finger with similarity to the *Drosophila* Polycomb group protein SU(Z)12 as well as *Arabidopsis* proteins FIS2 and EMF2 (*8*). In *vrn2* mutants, *FLC* expression is down-regulated normally in response to cold but, instead of remaining low, *FLC* RNA levels increase during later development at warm temperatures. *VRN2* thus functions to stably maintain *FLC* repression.

Another *Arabidopsis* mutant impaired in its response to vernalization is *vrn1* (*7*). Under our long-day growth conditions, plants with mutant *vrn1* alleles (*vrn1-1* ethylmethane sulfonate–induced, *vrn1-2* γ-ray induced) were not delayed in flowering but had a reduced vernalization response (Fig. 1, A and B). We conducted a detailed examination of *FLC* mRNA levels in *vrn1-1* plants to determine whether *FLC* repression was altered. In both *fca-1* and *vrn1-1 fca-1* plants, 6 weeks of cold temperature reduced *FLC* mRNA levels. In *vrn1-1 fca-1*, unlike *fca-1*, *FLC* levels increased again after transfer to normal growth temperatures (fig. S1). Therefore, *VRN1*, like *VRN2*, is required not for the initial down-regulation of *FLC* by cold but for stable maintenance of *FLC* repression during later development in warm temperatures.

We cloned the *VRN1* gene by a map-based approach (figs. S2 to S4). *VRN1* encodes a protein of 341 residues comprising two putative B3 DNA binding domains, originally described in the maize transcription factor VIVIPAROUS1 (VP1) (*9*); two predicted PEST regions involved in proteasome-dependent protein degradation (*10*); and a putative nuclear localization signal (Fig. 1C; figs. S4, S5). Analysis of a GFP-VRN1 chimeric protein in onion epidermal cells showed that VRN1 was nuclear localized (fig. S6).

VRN1 mRNA was detected at moderate levels in different tissues and developmental stages (Fig. 2, A and B) and was undetectable in *vrn1-1 fca-1* and *vrn1-2 fca-1* (Fig. 2C); as with *VRN2* (*8*), *VRN1* RNA levels were unaffected by vernalization (Fig. 2D). Rat polyclonal antibodies were raised against the NH_2-terminal 192 amino acids of VRN1 produced in *Escherichia coli*. VRN1 protein was detected at equivalent levels in wild-type and *fca-1* plants, was not detected in *vrn1-1 fca-1* and *vrn1-2 fca-1* seedlings (Fig. 2E), and was unaffected by 6 weeks of cold (Fig. 2F). The role of two predicted PEST regions in the VRN1 sequence thus remains unclear. The 53 res-

Department of Cell and Developmental Biology, John Innes Centre, Colney Lane, Norwich NR4 7UH, UK

*These authors contributed equally to this work.
†Present address: Laboratoire de Recherche Moléculaire sur les Antibiotiques, 15 rue de l'Ecole de Médecine, 75006 Paris, France.
‡Present address: Department of Botany, La Trobe University, Bundoora, Victoria, 3083, Australia.
§To whom correspondence should be addressed. E-mail: caroline.dean@bbsrc.ac.uk

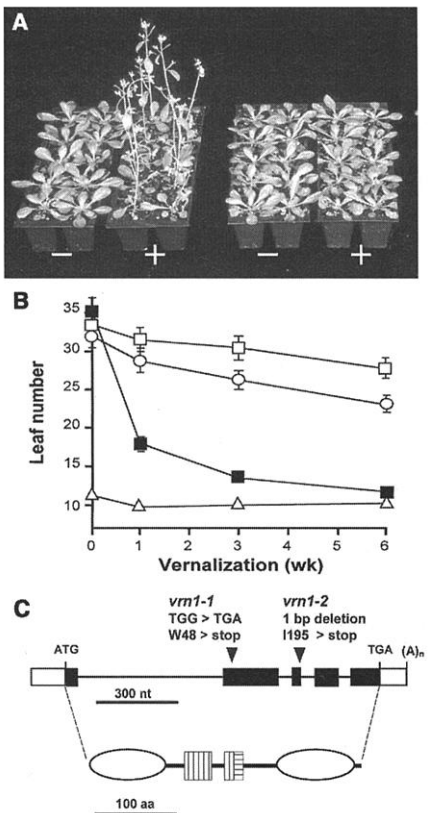

Fig. 1. Phenotype of *vrn1* mutant plants and structure of *VRN1* gene and encoded protein. **(A)** Plants (*fca-1*, left; *vrn1-1 fca-1*, right) were grown for 28 days under long-day photoperiods at 20°C, without (−) or with (+) 6 weeks of vernalization. **(B)** Vernalization dose-response curves. Landsberg *erecta* (open triangles), *fca-1* (closed squares), *vrn1-1 fca-1* (open squares), and *vrn1-2 fca-1* (open circles) were vernalized for 0, 1, 3, or 6 weeks before transfer to growth in long days at 20°C. Flowering time was scored as total leaf number (mean ± SE) (for 20 plants) for each genotype/treatment. **(C)** Structure of the *VRN1* gene (upper) and protein (lower). Exons are shown as black boxes and introns are shown as lines; the predicted translation start (ATG), stop (TGA), and polyadenylation [(A)n] sites are indicated; untranslated regions are boxed in white. Mutations in the *vrn1* alleles are indicated by arrowheads. Ellipses indicate B3-like domains; vertical hatches; PEST-like sequences; and horizontal hatches, nuclear localization signals. See fig. S3 and GenBank accession numbers AF289051 and AF289052 for details of the *VRN1* gene and transcript.

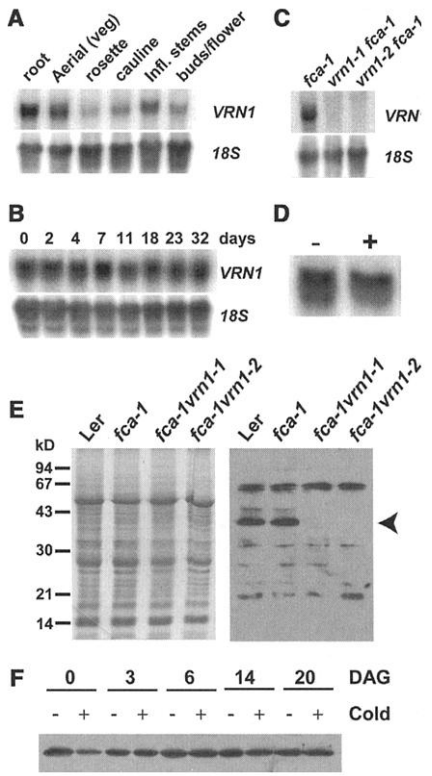

Fig. 2. Abundance of *VRN1* RNA and protein during development and in response to vernalization: northern analysis of *VRN1* RNA from *fca-1* tissues **(A)**, *fca-1* seedlings of different ages **(B)**, *fca-1* and *vrn1* mutants **(C)**, and *fca-1* seedlings without (−) or with (+) 6 weeks of vernalization **(D)**. Equal amounts of total RNA were loaded per lane as judged by ethidium bromide staining and reprobing the blot with 18S rDNA. **(E)** Immunoblot analysis of VRN1 protein from 14-day-old seedlings of different genotypes. Twenty micrograms of total protein was loaded on a SDS–12% polyacrylamide gel and stained with Coomassie blue (left) or blotted and probed with a rat VRN1 polyclonal antiserum diluted 1:2000 (right). Arrowhead indicates VRN1 protein. No truncated form of VRN1 was detected with the extracts prepared from *vrn1-1 fca-1* or *vrn1-2 fca-1*. **(F)** Immunoblot analysis of VRN1 protein from *fca-1* seedlings harvested 0, 3, 6, 14, or 20 days after germination (DAG) without (−) or with (+) vernalization.

idues encompassing the two PEST regions have an overall acidic charge (pI = 3.8 versus about 9.2 for the whole protein), so this region may play a role in transcriptional activation, as suggested for a similar region in ARF1, another B3-containing protein (*11*, *12*).

We fused *VRN1* to the strong cauliflower mosaic virus *35S* promoter (*13*, *14*) and transformed it into *vrn1-2 fca-1* plants. The most striking phenotype caused by the *35S::VRN1* transgene was early flowering without vernalization (Table 1, Fig. 3A). When *35S::VRN1* plants were vernalized before growth, flowering was further accelerated (Table 1). Under noninductive short-day conditions, the *35S::VRN1* plants flowered later than under long photoperiods, and vernalization accelerated flowering (Table 1). This retention of photoperiod response in *35S::VRN1* plants suggests that *VRN1* is not functioning through the photoperiod pathway. The *35S::VRN1* plants showed additional morphologic phenotypes compared with control plants, including reduced flower abscission, a less acute angle between the siliques and the inflorescence stem, shortened pedicles (Fig. 3B), more variable and flattened silique shape (Fig. 3C), and a looser flower structure with somewhat enlarged petals (Fig. 3D). These characteristics suggest that *VRN1* functions more broadly than vernalization. The role of *VRN1* in vernalization-independent flowering control is also revealed when loss-of-function mutants are grown in different conditions (*4*). In 16-hour high-light photoperiods [with a red/far-red (R/FR) ratio of 2.3], *vrn1* mutants do not flower late (Fig. 1B); however, in extended short-day (ESD) conditions (*15*), in which the long photoperiod is composed of 10 hours of high light (R/FR ratio of 2.3) and 6 hours of low-intensity incandescent light (R/FR ratio of 0.66), *vrn1* is late flowering (Table 1).

To investigate the molecular basis of the acceleration of flowering by *35S::VRN1* and the vernalization-independent function of *VRN1*, we examined the expression of *FLC*, *AGL20*, and *FT*. The abundance of *AGL20* and *FT* RNA was increased in *35S::VRN1* plants compared with wild-type and empty vector control plants (Fig. 3, E and F). One possible cause of elevated expression of *FT* and *AGL20* in *35S::VRN1* plants is an enhancement of *VRN1* repression of *FLC*. However, *FLC* RNA levels were unchanged in *35S::VRN1* plants compared with controls (Fig. 3, E and G). Therefore, the accelerated flowering of *35S::VRN1* lines under long- and short-day photoperiods without vernalization (Table 1) is through a pathway that does not regulate *FLC* RNA levels but does activate *AGL20* and *FT*, targets of multiple floral pathways (Fig. 3J). Vernalization causes additional earliness in *35S::VRN1* lines due to down-regulation of *FLC* RNA by vernalization (Fig. 3G). To investigate the consequences of ectopic *FT* and *AGL20* expression, we introduced *ft-7* and *soc1* (a loss-of-function *AGL20* allele) mutations into the *35S::VRN1* line 6C introgressed into Landsberg *erecta* (*Ler*). In greenhouse conditions, *soc1* ameliorated the phenotype of the *35S::VRN1* lines only slightly, whereas *ft-7 35S::VRN1* lines flowered late (with between 19 and 23 leaves), similar to *ft-7*. Therefore, in these conditions, the early flowering of *35S::VRN1* is mainly due to ectopic expression of *FT*. Consistent with

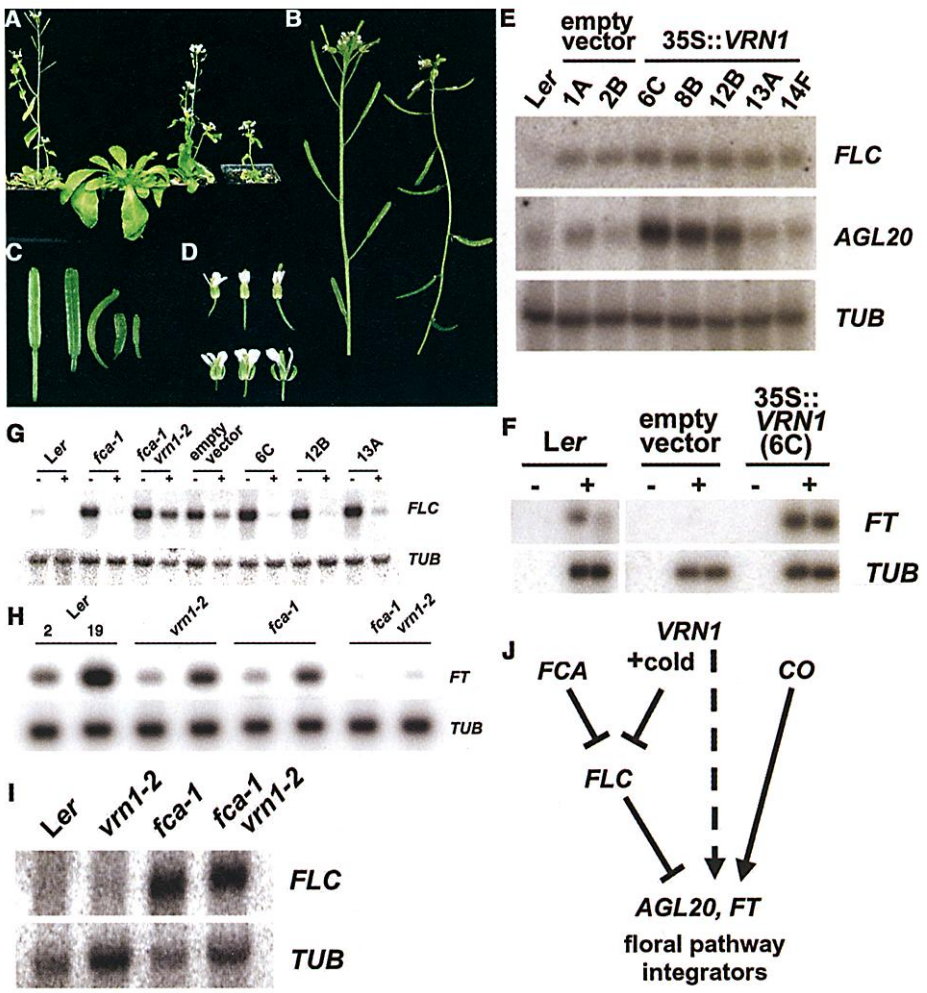

Fig. 3. Phenotypes of transgenic plants overexpressing *VRN1*. (**A**) Plants (21 days old) grown in ESD without vernalization. Left to right: wild-type, vrn1-2 *fca-1* empty vector, two *35S::VRN1 vrn1-2 fca-1* lines, 13A and 12B (all Landsberg *erecta* background). (**B**) Compared with wild-type (left), *35S::VRN1* (right) inflorescences showed a less acute angle between the siliques and the pedicles and a defect in floral organ abscission. (**C**) Silique morphology of *35S::VRN1* lines (right) was variable compared with wild type (left). (**D**) Flowers of overexpressing lines (lower) were larger than those from the parental line (*vrn1-2 fca-1*) (upper) and had a looser structure. (**E**) Northern blot analysis of *FLC* and *AGL20* expression. Seedlings were grown without vernalization and harvested after 7 days. Total RNA samples were hybridized with gene-specific probes as described in (*5*, *8*). β-Tubulin (*TUB*) mRNA served as a loading control. (**F**) Effect of *35S::VRN1* transgene on *FT* expression was investigated by reverse transcriptase PCR (RT-PCR), as described in (*20*, *21*), on RNA prepared from 7-day-old nonvernalized seedlings. Duplicate samples were reverse transcribed [without (−) or with (+) enzyme] and hybridized with *TUB*- or *FT*-specific probes. (**G**) Northern blot analysis of *FLC* and *TUB* expression in line *35S::VRN1* 6C with and without vernalization. (**H**) RT-PCR analysis of *FT* and *TUB* expression in loss-of-function *vrn1-2* seedlings grown for 3 weeks in ESD and harvested 2 and 19 hours after dawn. (**I**) Northern blot analysis of *FLC* and *TUB* expression in loss-of-function *vrn1-2* seedlings grown in ESD. (**J**) Model for multiple roles of *VRN1* in controlling the floral transition. In the vernalization response, VRN1 in association with cold-induced factors maintains repression of *FLC*. *VRN1* also acts in a pathway that does not affect *FLC* RNA levels but positively regulates *AGL20* and *FT*. This is drawn as an independent pathway to the photoperiod pathway, as *35S::VRN1* plants flower later in short days and their flowering is further accelerated by vernalization.

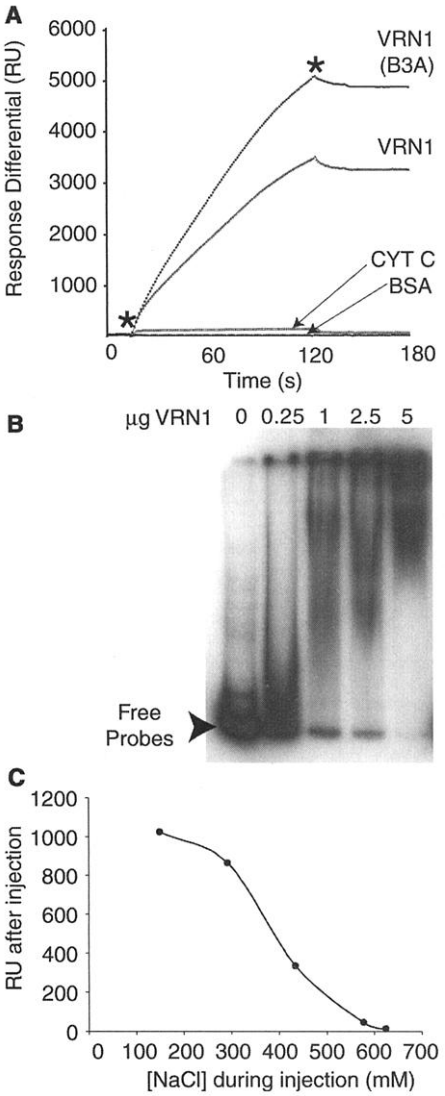

Fig. 4. VRN1 protein binds to DNA in a non–sequence-specific manner in vitro. (**A**) BIACORE SPR sensorgrams (www.biacore.com) showing the binding of protein (equal 5-µg amounts) to a double-stranded DNA (140 bp) fragment from pBR322 immobilized on a SA chip. Asterisks mark beginning and end of DNA injections. VRN1 protein and the first B3 domain alone (VRN1 B3A) bind strongly compared with horse heart cytochrome c (CYT C) (similar overall pI to VRN1) and bovine serum albumin (BSA). (**B**) Typical electrophoretic mobility shift from VRN1 binding to an *FLC* fragment. VRN1 protein (0 to 5 µg), poly(dIdC) (2 µg), bovine serum albumin (6 µg), and a 360-bp radiolabeled double-stranded *FLC* probe (10,000 cpm) were incubated at room temperature for 30 min in 100 mM KCl, 10 mM Hepes·OH (pH 7.9), 1 mM EDTA, 10 mM $MgCl_2$, 10% glycerol, 1 mM dithiothreitol and then separated on an 8% tris-borate EDTA–polyacrylamide gel. (**C**) DNA binding by VRN1 is salt dependent. Spiking 10-µmol injections of *FLC* DNA fragment 8 with increasing amounts of NaCl reduced the ability of the DNA to bind VRN1. Because SPR is affected by the addition of salt, the amount of DNA bound to the chip after the injection (RU after injection) was plotted.

Table 1. Effects of mutations and transgenes on flowering time of plants under different conditions [ESD, extended short-day, and SD, short-day photoperiods; V, 5 weeks of vernalization (*15*)]. Flowering time is recorded as mean total leaf number at flowering ± SE. At least 10 plants were counted unless indicated.

Genotype	ESD–V	+/–	ESD+V	+/–	SD–V	+/–	SD+V	+/–
Ler	8.7	0.2	9.1	0.1	47.3	0.5	30.6	0.6
vrn1-2	11.7	0.4	13.7	0.3	40.5	1.0	42.3	0.9
fca-1	35.6	0.5	10.9	0.2	68.0	1.8	31.8	0.7
vrn1-2 fca-1	46.7	1.3	22.1	0.6	66.8	2.3	55.3	2.3
35S::VRN1 6C *vrn1-2 fca-1*	11.6	0.3	7.7	0.1	44.0	0.7	17.8	0.2
35S::VRN1 12B *vrn1-2 fca-1*	11.3	0.2	8.8	0.2	42.6*	0.8	17.4	0.2
35S::VRN1 13A *vrn1-2 fca-1*	20.4	0.7	10.4	0.2	54.0†	1.3	26.5	0.5

*Nine plants. †Six plants.

this, *vrn1-2* plants in ESD conditions showed reduced *FT* but wild-type *FLC* expression (Fig. 3, H and I).

So far, we have found no interaction of VRN1 and VRN2 by using yeast two-hybrid assays, so whether they function as part of the same multisubunit complex remains an open question. With electrophoretic mobility shift assays and surface plasmon resonance (SPR), we have pursued whether VRN1 could act in recruiting a protein complex to the *FLC* locus by investigating whether VRN1 specifically binds to *FLC*. Soluble *E. coli* expressed histidine-tagged and untagged whole VRN1 protein bound to 27 *FLC* fragments in a salt- and concentration-dependent manner (Fig. 4, fig. S7). The *FLC* fragments used represented 95% of the *FLC* genomic region [beginning 1856 base pairs (bp) upstream of the ATG codon and ending 695 bp downstream of the translation stop codon, containing all noncoding sequence and some of the exon sequences] (table S1, fig. S7). We observed the strong non–sequence-specific interaction for VRN1 with a wide range of unrelated DNA sequences from *Arabidopsis VRN2*, *AGL20*, and *TUB* and *E. coli GyrB* as well as pBR322 and the DNA polynucleotide poly(dIdC). Such in vitro non–sequence-specific DNA binding has been observed for Polycomb/trithorax group proteins (*16*) and high mobility group box (HMG-box) proteins, including the *Arabidopsis* FILAMENTOUS FLOWER protein, which is involved in meristem and organ identity (*17*). However, in vivo many proteins showing in vitro DNA binding activity are targeted to specific genomic regions (*18*). An important issue is to identify the range of VRN1 targets in vivo and to address whether VRN1 regulates *FLC*, *FT*, and *AGL20* directly. *FLC* and *FT* appear to be regulated by changes in chromatin structure (*8*, *19*), so the non–sequence-specific DNA binding of VRN1 is consistent with it being a component of many multisubunit complexes involved in chromatin regulation. Another important issue to address is the nature of the vernalization-specific factors required to specify *FLC* as a target of VRN1. Cold-induced posttranslational modifications of VRN1 and changes in cellular location may change VRN1 activity. Alternatively, vernalization-induced accessory proteins may recruit VRN1 into a complex, possibly including VRN2, that can target *FLC*.

References and Notes

1. G. G. Simpson, C. Dean, *Science* **296**, 285 (2002).
2. S. D. Michaels, R. M. Amasino, *Plant Cell* **11**, 949 (1999).
3. C. C. Sheldon *et al.*, *Plant Cell* **11**, 445 (1999).
4. C. C. Sheldon, D. T. Rouse, E. J. Finnegan, W. J. Peacock, E. S. Dennis, *Proc. Natl. Acad. Sci. U.S.A.* **97**, 3753 (2000).
5. A. Samach *et al.*, *Science* **288**, 1613 (2000).
6. H. Lee *et al.*, *Genes Dev.* **14**, 2366 (2000).
7. J. Chandler, A. Wilson, C. Dean, *Plant J.* **10**, 637 (1996).
8. A. R. Gendall, Y. Y. Levy, A. Wilson, C. Dean, *Cell* **107**, 525 (2001).
9. M. Suzuki, C. Y. Kao, D. R. McCarty, *Plant Cell* **9**, 799 (1997).
10. M. Rechsteiner, S. W. Rogers, *Trends Biochem. Sci.* **21**, 267 (1996).
11. T. Ulmasov, J. Murfett, G. Hagen, T. J. Guilfoyle, *Plant Cell* **9**, 1963 (1997).
12. S. J. Triezenberg, *Curr. Opin. Genet. Dev.* **5**, 190 (1995).
13. The VRN1 open reading frame from EST F2H7 was polymerase chain reaction (PCR)–amplified with TTTTTTCATATGCCACGCCCTTTCTTCCATAAGTTGATTTTC and GGCAACTCGAGTAGTTAATCAGACGTACTCGTTGACTCGAAAGGCTG.
14. J. S. Mylne, J. R. Botella, *Plant Mol. Biol. Rep.* **16**, 257 (1998).
15. J. H. Clarke, R. Mithen, J. K. M. Brown, C. Dean, *Mol. Gen. Genet.* **248**, 278 (1995).
16. J. A. Simon, J. W. Tamkun, *Curr. Opin. Genet. Dev.* **12**, 210 (2002).
17. E. Kanaya, N. Nakajima, K. Okada, *J. Biol. Chem.* **277**, 11957 (2002).
18. G. J. Narlikar, H.-Y. Fan, R. E. Kingston, *Cell* **108**, 475 (2002).
19. M. Blazquez, M. Koornneef, J. Putterill, *EMBO Rep.* **2**, 1078 (2001).

20. I. Kardailsky *et al.*, *Science* **286**, 1962 (1999).
21. Y. Kobayashi, H. Kaya, K. Goto, M. Iwabuchi, T. Araki, *Science* **286**, 1960 (1999).
22. We thank L. Mitchenall and N. Burton for their efforts in producing VRN1 protein; M. Wall and C. Noble for help with BIACORE; P. Buckle for BIACORE analysis; T. Maxwell for helpful discussions; and M. Smith for excellent care of *Arabidopsis* plants. Supported by a U.K. Biotechnology and Biological Sciences Research Council grant to C.D.; a Core Strategic Grant to the John Innes Centre; European Commission grants to C.D.; and an EMBO long-term fellowship to S.M.

Supporting Online Material
www.sciencemag.org/cgi/content/full/297/5579/243/DC1
Figs. S1 to S7
Table S1

22 March 2002; accepted 12 June 2002